crystals

MDPI

Article

Strengthening and Thermally Activated Processes in an AX61/Saffil Metal Matrix Composite

Zuzanka Trojanová [1,2], Zoltán Száraz [1,3], Pavel Lukáč [1,2], Zdeněk Drozd [1,*] and Ján Džugan [2]

1 Faculty of Mathematics and Physics, Charles University, Ke Karlovu 3, 121 16 Praha 2, Czech Republic; ztrojan@met.mff.cuni.cz (Z.T.); Zoltan.SZARAZ@ec.europa.eu (Z.S.); lukac@met.mff.cuni.cz (P.L.)
2 Comtes FHT, Průmyslová 996, 334 41 Dobřany, Czech Republic; jdzugan@comtesfht.cz
3 Directorate G—Nuclear Safety and Security, Joint Research Center, Westerduinweg 3, NL-1755ZG Petten, The Netherlands
* Correspondence: zdenek.drozd@mff.cuni.cz

Received: 16 April 2020; Accepted: 13 May 2020; Published: 1 June 2020



Abstract: AX61 magnesium alloy was reinforced with short Saffil fibres using squeeze cast technology. Samples were cut from the casting in two directions: parallel and perpendicular to the fibre plane. Samples were deformed in compression at various temperatures from room temperature to 300 °C. Various strengthening mechanisms such as load transfer, increased dislocation density, Orowan and Hall–Petch strengthening were analysed. During deformation, the stress relaxation tests were subsequently performed. The relaxation curves were evaluated with respect to Li and Feltham equations with the aim to find stress components in matrix and parameters of the thermally activated process(es).

Keywords: AX61 magnesium alloy; compressive deformation; stress relaxation; thermally activated processes; composite strengthening

1. Introduction

In the last few decades, magnesium alloys have been the focus of designers because of their high specific stiffness, strength and wear resistance [1]. The Mg-Al-Ca (AX) alloys were developed as creep-resistant alloys designated for applications at elevated temperatures. Ca serves as a cheaper substitute of rare earth elements and for microstructure refinement [2–12]. Good thermal stability of the second phase particles is the main reason for the good mechanical properties at higher temperatures. Microstructure and phase selection depend on Ca/Al mass ratio. If this ratio Ca/Al < 0.8, formation of $Mg_{17}Al_{12}$ with the low eutectic temperature of 437 °C is supressed and good mechanical properties at elevated temperatures may be ascribed to the $(Mg, Al)_2Ca$ particles with an eutectic temperature of 517 °C and melting point of 710 °C [4,13–15]. Recently, Elamami and co-workers studied microstructure and phase selection in Mg-Al-Ca-Mn cast alloys with Ca/Al ratios from 0.58–0.91 [8]. The detailed analysis showed that Mg-Al-Ca alloys contain various second phases of Laves type depending on Ca/Al ratios and thermal treatment [16]. Further improvement of mechanical properties is possible using some method of severe plastic deformation [17–20]. These methods, such as equal channel angular pressing (ECAP), high pressure torsion (HPT) or repetitive corrugation and straitening (RCS), are not yet able to prepare bigger work-pieces of a material. The addition of ceramic, graphite or metallic micro- and nano(particles/fibers/whiskers/tubes) as reinforcement into ductile matrix may significantly improve module, strength or fatigue resistance [21–27]. On the other hand, the ductility of such composites rapidly decreases with increasing volume fraction of the reinforcing phase. The possible use of other strengthening procedures, such as severe plastic deformation, is, in the case of metal matrix

composites (MMCs) based on magnesium alloys, strongly limited [28–31]. Deeper understanding of strengthening mechanisms and behaviour of dislocations in the composite matrix can help to extend applications opportunities of magnesium-based metal matrix composites.

The strengthening effect of fibres, i.e., the difference between the stress necessary for deformation of the composite and the unreinforced matrix alloy, is a complex magnitude containing various contributions:

- load transfer of the applied stress to the well bonded fibres ($\Delta\sigma_{LT}$) [32];
- generation of thermal dislocations due to a significant difference between the thermal expansion coefficient ($\Delta\alpha$) of metallic matrix and ceramic fibres ($\Delta\sigma_{CTE}$) [33];
- dislocations geometrically necessary that are crated in order to accommodate large strain gradient and allowing compatible deformation ($\Delta\sigma_{GEO}$) [34];
- Hall–Petch strengthening due to finer grain structure in the composite compared with the unreinforced alloy ($\Delta\sigma_{HP}$);
- Orowan strengthening ($\Delta\sigma_{OR}$) [35];
- residual thermal stresses in the matrix ($\Delta\sigma_{TH}$) [36].

In a composite material, plastic deformation occurs in the matrix while particles or fibres of the second phase deform only elastically. The resolved shear stress in response to plastic deformation is related to densities and interactions of dislocations with obstacles existing in the slip plane. The stress necessary for dislocation motion in the slip plane, τ, can be divided into two components:

$$\tau = \tau_i + \tau^*, \tag{1}$$

where τ_i is the internal (athermal) stress, the critical resolved shear stress needed to move dislocation through the stress field of long range obstacles, which represent dislocations in various slip systems

$$\tau_i = \alpha_1 Gb\rho_t^{1/2}, \tag{2}$$

where α_1 is a constant reflecting interaction between dislocations, G is the shear modulus, b is the magnitude of Burgers vector and ρ_t is the total dislocation density. τ^* is the effective (thermal) stress necessary to overcome local obstacles with the help of thermal activation (due to lattice vibrations). If mobile dislocations with a density of ρ_m move through local obstacles in slip plane with an average velocity, $\overline{v}$, a strain rate, $\dot{\gamma}$, may be expressed according to Orowan [37] as

$$\dot{\gamma} = \rho_m \overline{v}\ b, \tag{3}$$

$$\text{with } \overline{v} = \dot{\gamma}_0 \exp\left[-\frac{\Delta G(\tau^*)}{kT}\right], \tag{4}$$

where $\dot{\gamma}_0 = \beta bv$ with the model dimensionless constant β, ν is an attempt frequency and kT has its usual meaning. The Gibbs free enthalpy depends on the effective stress $\tau^* = \tau - \tau_i$ and its simplest form is:

$$\Delta G(\tau^*) = \Delta G_0 - V\tau^* = \Delta G_0 - V(\tau - \tau_i), \tag{5}$$

where ΔG_0 is the Gibbs free enthalpy necessary for overcoming a short-range obstacle without the stress and V is the activation volume. In polycrystalline materials, the applied stress σ is related to the resolved shear stress τ and its corresponding components by the Taylor factor M: $\sigma = M\tau$. Then, the applied stress, σ, necessary for deformation of polycrystals is usually divided into two components:

$$\sigma = \sigma_i + \sigma^*. \tag{6}$$

Correspondingly,

$$\dot{\varepsilon} = 1/M\dot{\gamma} \tag{7}$$

Decomposition of the flow stress into two components may be performed experimentally. The activation volume, V, may be expressed as $V = bd\ell$, where d is the obstacle width and ℓ effective length of dislocation segments between local obstacles. The product $A = d\ell$, is an activation area overlapped with the dislocation segment of the length, ℓ, after successful activation.

In this study, an analysis of the thermally activated processes was performed using stress relaxation testing was performed with the aim to find the main thermally activated processes occurring during plastic deformation of an AX61 magnesium alloy reinforced with 26 vol% of short Saffil fibres. The reinforcing effect of fibres was analysed and the main strengthening mechanism evaluated.

2. Materials and Methods

AX61 alloy (nominal composition: 6 wt.% Al-1 wt.% Ca-balance Mg) was used as the matrix alloy. The alloy was reinforced with δ-Al_2O_3 short fibres (Saffil) with a mean diameter of 3 μm and a mean length about 87 μm (measured after squeeze casting). MMC was prepared by the squeeze casting method. The preform consisting of Al_2O_3 short fibres and showing a planar isotropic fibre distribution and a binder system (containing Al_2O_3 and starch) were preheated to a temperature higher than the melt temperature of the alloy and then inserted into a preheated die to 360 °C. The preform was preheated to a temperature higher than the melting temperature of the alloy (to avoid solidification during the infiltration process). The melt was superheated to between 700 and 720 °C and poured over the preform. The vertical stamp squeezes the melt with a pressure of approximately 60 MPa into the preform and the solidification takes approximately one minute. After the infiltration, the solidification process occurs under the pressure which leads to the fine microstructure without porosity and residual gases. The two-stage application of the pressure resulted in MMCs with a fibre volume fraction of 26 vol.% fibres. The real content of fibres was estimated by the hydrostatic weighting to be in the range of 25.7–25.9 vol.% of Saffil.

Samples for deformation tests with the geometry of $5 \times 5 \times 10$ mm^3 were cut from the composite casting so that the stress axis was either parallel (par) or perpendicular (per) to the fibres plane. Samples of both orientations were deformed in compression in an Instron 1186 machine with an initial strain rate of 2.4×10^{-5} s^{-1} at temperatures from room temperature to 300 °C. The true stress–true plastic strain curves were calculated from force-shortening dependences. For compression tests, three samples were used. Stresses were measured with the standard deviation of 5%. Sequential stress relaxation (SR) tests were performed so that the sample was deformed to a certain stress, σ_0, and then the machine was stopped and the stress decrease depending on time was recorded. Subsequently, (after 300 s) the specimen was reloaded and deformed to a higher stress (strain) and the relaxation was repeated.

The SR experiment allowed us to estimate the activation volume, V. In the literature, there are various possibilities of how to calculate the activation volume [38,39] from the SR. For our experiments, the Feltham equation [39] was the most suitable; the stress decrease with time during the SR can be described as

$$\Delta\sigma(t) = \sigma(0) - \sigma(t) = \alpha_2 \ln(\beta t + 1), \tag{8}$$

where $\sigma(0) \equiv \sigma_0$ is the stress at the beginning of the stress relaxation at time $t = 0$, $\alpha_2 = kT/V$ and

$$\beta = \frac{S\dot{\varepsilon}(0)}{\alpha}, \tag{9}$$

where S is the machine stiffness and $\dot{\varepsilon}(0) = \dot{\gamma}(0)/M$ is the plastic strain rate at the beginning of the relaxation. The SR tests enabled us to estimate to separate the internal stress, σ_i, and effective stress, σ^*. The SR curves were fitted to the power law function in the form [40,41]

$$\sigma - \sigma_i = [a(m-1)]^{1/1-m}(t + t_0)^{1/1-m}, \tag{10}$$

In Equation (10), a, m and t_0 are the fitting parameters.

3. Results

The microstructure of the squeeze cast matrix alloy is shown in Figure 1. Due to the low solubility of Ca, particles of the second phase are formed mainly in the grain boundaries. Chemical analysis revealed that these precipitates are Al_2Ca intermetallic compounds.

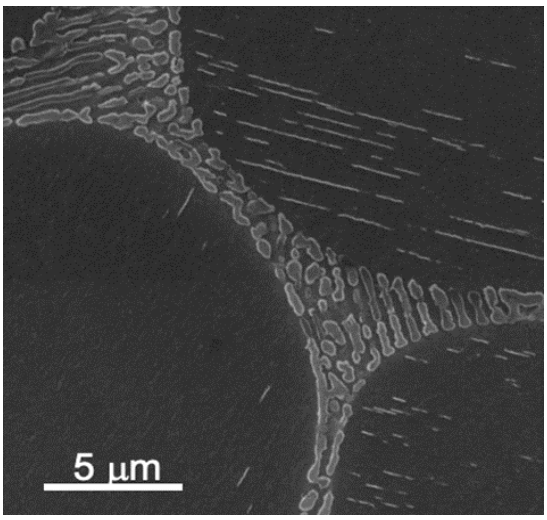

Figure 1. Electron micrograph of the AX61 alloy showing particles in grain boundaries.

Figure 2 shows fibre distribution in the section parallel to the fibres plane (Figure 2a) and perpendicular to the fibres plane (Figure 2b). The fibres distribution is not ideal. During the squeeze casting, the planar random distribution was partially destroyed.

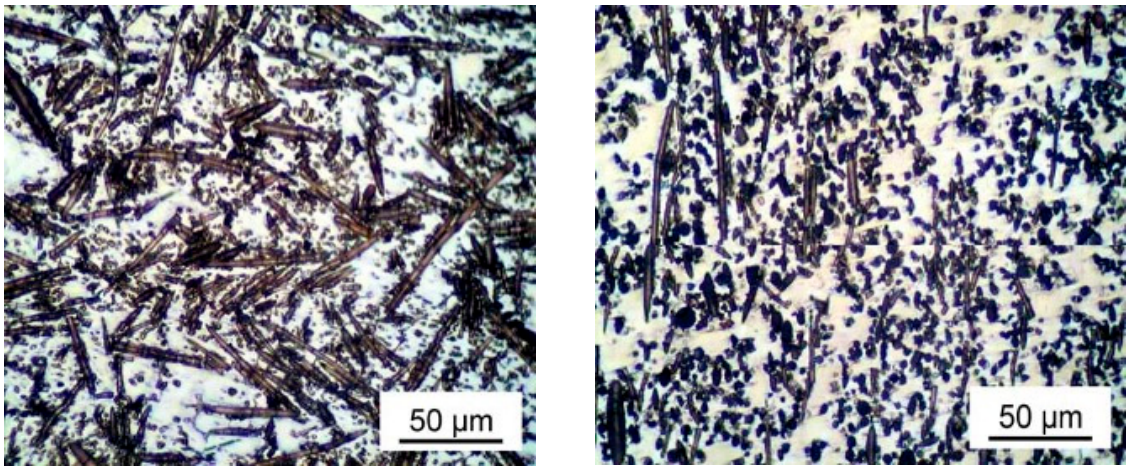

(**a**) (**b**)

Figure 2. Light micrograph showing Saffil fibres: (**a**) section parallel to the fibre plane; (**b**) section perpendicular to the fibre plane.

The stress–strain curves of samples with parallel orientation of the fibres plane were estimated at various temperatures (Figure 3a). Corresponding curves found for samples with the perpendicular orientation are shown in Figure 3b. Deformation stress of both sample orientations decrease with increasing temperature. Note that in this case, no SR tests were performed during the deformation test. It is evident that deformation stresses estimated for samples with parallel orientation are much lower compared with ones found for samples with perpendicular orientation. On the other hand, the ductility of perpendicular samples is higher.

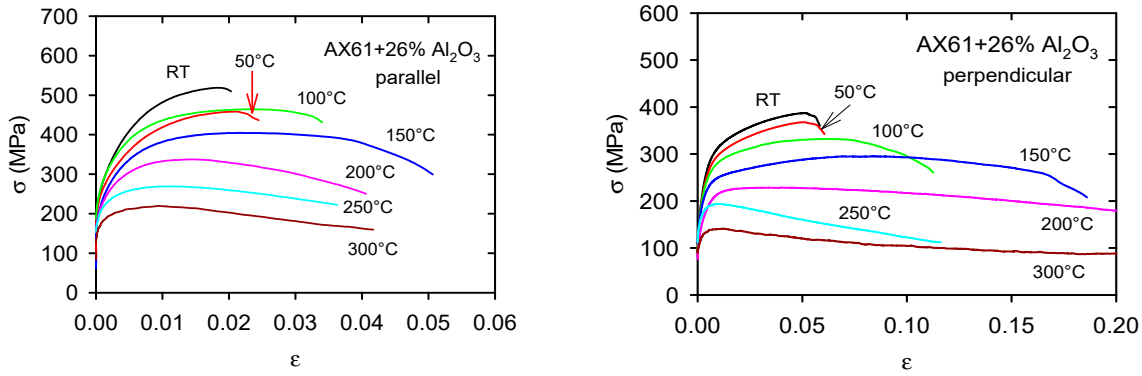

(**a**) (**b**)

Figure 3. Stress–strain curves obtained at various temperatures estimated for (**a**) samples with parallel orientation and (**b**) for samples with perpendicular orientation.

The temperature dependences of the yield, σ_{02}, and maximum, σ_{max}, stresses are displayed in Figure 4. For comparison, values for unreinforced alloy were added. It is obvious that the strengthening effect of fibres is huge, especially for samples with the parallel orientation.

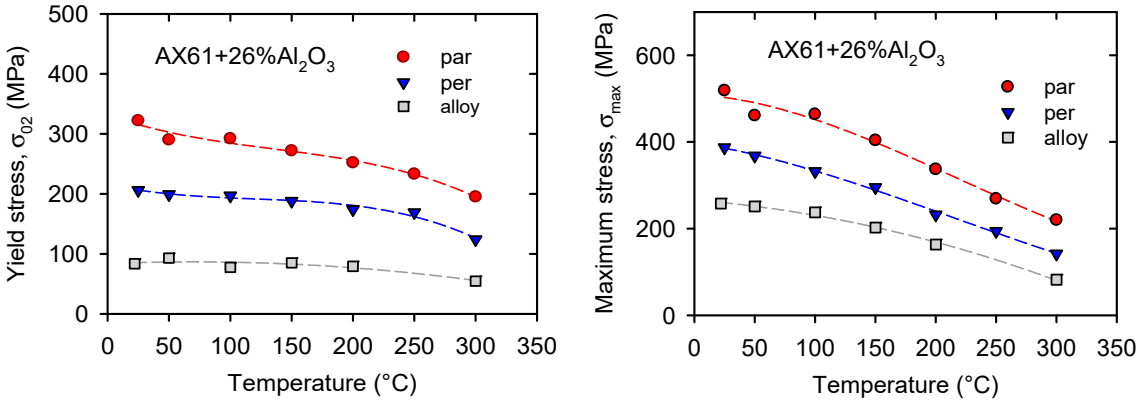

(**a**) (**b**)

Figure 4. Temperature dependence of the (**a**) yield stress and (**b**) maximum stress obtained for samples with both fibre orientations.

Examples of the SR curves obtained at 100 °C for samples of both fibre orientations are shown in Figure 5a,b. The curves in Figure 5 are normalized, i.e., $\sigma(t)/\sigma(0)$ values are plotted against time, t.

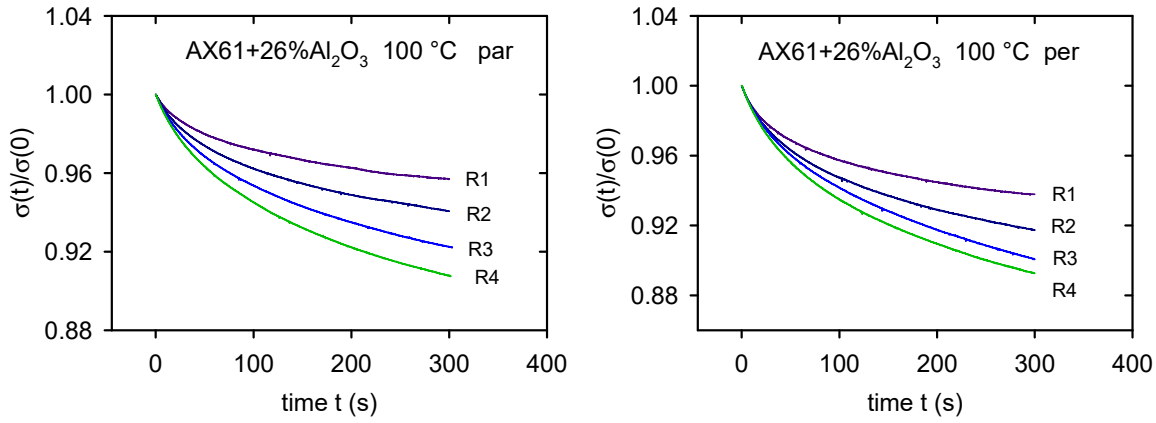

(**a**) (**b**)

Figure 5. Sequence of stress relaxation (SR) curves estimated during deformation at 100 °C of (**a**) parallel and (**b**) perpendicular fibres orientation.

4. Discussion

4.1. Strenghtening Influence of Fibres

The yield stress values obtained for both fibre orientations decrease with temperature up to 250 °C relatively slowly. This result is beneficial for the high-temperature application of these composites. The reinforcing effect of fibres is obvious from Figure 4 comparing the temperature dependence of the yield stresses obtained for the unreinforced alloy and the alloy with fibres. From Figure 4 it is clear to see that the reinforcing influence of fibres is more effective for the composite with the parallel orientation of the fibres plane. The fibres effect on strengthening is affected by the geometry of fibres and their orientation to the stress direction. The yield stress increases, ($\Delta\sigma_C = \sigma_C(\text{par}) - \sigma_A$, σ_A is the alloy yield stress), exhibiting ~230 MPa at room temperature compared with the unreinforced alloy prepared with the same technology, i.e., squeeze casting. The reinforcing effect of fibres decreases with increasing temperature up to 140 MPa at 300 °C.

The relationships which may be used for calculations of individual strengthening terms are summarized in Table 1. The meaning of quantities used in equations reported in Table 1 are explained in Table 2.

Table 1. Individual contributions to strengthening following from the presence of the reinforcing phase.

Mechanism	Relationship
Load transfer	$\sigma_{LT} = \sigma_A\left[1 + \frac{(L+t)\chi}{4L}\right]f + \sigma_A(1-f)$
Thermal mismatch	$\rho_T = \frac{Bf\Delta\alpha\Delta T}{b(1-f)}\ \frac{1}{t}$
Enhanced dislocation density	$\Delta\sigma_D = \alpha_1\ \psi Gb(\rho_T + \rho_G)^{1/2}$
Geometrical dislocations	$\rho_G = \frac{f8\varepsilon_p}{bt}$
Orowan strengthening	$\Delta\sigma_{OR} = \frac{Gb}{\Lambda} + \frac{5}{2\pi}Gf\varepsilon_p$
Residual stresses	$\langle\sigma_m\rangle_{max} = \frac{2}{3}\sigma_y In\left(\frac{1}{f}\right)\frac{1}{1-f}$
Hall-Petch strengthening	$\sigma_{GS} = K_y\left(d_2^{-1/2} - d_1^{-1/2}\right)$

Table 2. Meaning of the quantities introduced in Table 1.

σ_{LT}	ρ_T	ρ_G	σ_{OR}	$<\sigma_m>_{max}$	$\Delta\sigma_{GS}$	G
L fibre length, t fibre thickness, σ_A alloy stress, $\chi = L/t$	b Burgers vector, $B = 10$ for fibres, $\Delta\alpha\Delta T$ thermal strain	ε_p plastic strain f volume fraction of fibres	Λ distance between fibres	σ_y yield stress in the matrix	K_y Hall-Pech constant, d grain size	shear modulus

Various contributions to the composite strengthening were calculated for the yield stress, measured at room temperature, and introduced in Table 3. Parallel orientation of the fibre plane was considered for the estimation of the load transfer. For the calculations, the parameters shown in Table 4 were used. Note that σ_m in Table 3 is the sum of σ_A and the contribution resulting from the increased dislocation density in the matrix due to generation of thermal and geometrically necessary dislocations.

Table 3. Individual strengthening terms calculated for the yield stress.

σ_{LT} (MPa)	ρ_T (m^{-2})	ρ_G (m^{-2})	$\Delta\sigma_D$ (MPa)	σ_{OR} (MPa)	$<\sigma>_{max}$ (MPa)	$\Delta\sigma_{GS}$ (MPa)	σ_m (MPa)	σ_{exp} (MPa)	σ_{theor} (MPa)
95	4.8×10^{13}	4.3×10^{12}	63.3	3	48	20.4	153.3	322	320

Table 4. Parameters used for calculations according Table 2.

α (AX61) (K^{-1})	α (Saffil) (K^{-1})	G (GPa)	b [m]	Ky ($MPam^{-3/2}$)	Taylor Factor M	α_1
26×10^{-6}	6×10^{-6}	17	3.2×10^{-10}	10.5	4.6	0.35
this study	[42]			[43,44]	[45]	[46]

The stress increase due to the load transfer in the case of perpendicular orientation of the fibres plane is negligible $\Delta\sigma_{LT}$(per) = 5.6 MPa. Note that the relationship for the load transfer stress is constructed for the case where all fibres are parallel to the load direction. The AX61 composite exhibits 2D arrangement of fibres, i.e., only the fibre plane is parallel (or perpendicular) to the load direction. For the estimation of σ_{LT}, only a part of the calculated value $\eta\sigma_{LT}$ = 88 MPa was considered. Parameter $\eta = 0.6$ is the mean value of the direction cosines. Farkas et al. studied lattice microstrains appearing during the deformation of a similar composite, as in this study, using neutron diffraction [47]. They evaluated the load transfer from the matrix to fibres $\Delta\sigma_{LT}$~100 MPa by measuring the applied stress dependence of the {10.1} lattice strain. This is close to calculated value σ_{LT}^{theo} = 95 MPa. Note that relationships stated in Table 2 are constructed for the perfect bonding between the matrix and reinforcing phase. Although this condition is not fulfilled in all cases, the bonding between magnesium and Al_2O_3 fibres may be considered as strong [48,49].

The authors of [47] measured in situ residual thermal stresses in the matrix using neutron diffraction. They estimated relatively high value of ~100 MPa. Residual thermal stresses have tensile character and are reason for the tension compression asymmetry observed in composites [50]. In the compression test applied stress has to overcome residual tensile stresses existing in the matrix and then compressive deformation is realised. On the other hand, it is not possible to calculate the load transfer difference between the yield stresses obtained for tension and compression, because of distinct deformation mechanisms. Jiang and co-workers [51] developed an analytical model for the estimation of the yield stress in a composite reinforced with aligned short fibres. They found that the plastic deformation under tensile loading starts in the matrix around the fibres and the yielding is achieved at smaller stress. On the other hand, in compression, the composite yields early in the vicinity of fibre ends overall at higher stress. The residual stress significantly reduces the tensile yield strength.

The theoretical stress, necessary for compressive deformation, σ_{theor}, was calculated as a simple sum of individual strengthening terms. The question of how to combine these contributions was solved

in several studies. Clyne and Whitters [52] and Lilhold [53] suggested that the stress contributions, which act more or less uniformly throughout the matrix, may be superimposed linearly.

With increasing temperature, the stress in the matrix decreases and thereby the load transfer and residual thermal stresses. At temperatures higher than 200 °C, recovery mechanisms in the matrix may cause a decrease in the dislocation density and the deformation stresses. A decrease in the thermal dislocation density in magnesium alloys was experimentally observed in internal friction experiments [54].

4.2. Hardening in the Matrix

The observed decrease in the fibres strengthening effect with increasing temperature may have several reasons. Thermal stresses in the matrix decrease with increasing deformation temperature, thermal dislocations can be partially erased at elevated temperatures. Likewise, the bonding between the matrix and reinforcing phase, at room temperature strong, may be partially released at higher temperatures, as well. The thermally activated processes play an important role at elevated temperatures. Therefore, the stress necessary for composite deformation, σ_C, can be expressed as

$$\sigma_C = \sigma_{LT} + \sigma_{mi} + \sigma_m^*, \tag{11}$$

where σ_{mi} , σ_i^* are internal and thermal (effective) stress in the matrix and σ_{LT} is contribution of the load transfer. Decomposition of the matrix stress into two components σ_{mi} , σ_m^* was performed by fitting of experimental estimated stress relaxation data to Equation (10). Examples of such stress decomposition are shown in Figure 6a (parallel orientation) and b (perpendicular orientation) for curves obtained at 100 °C. A part of the stress–strain curve obtained for composite was divided into three curves: stress in the matrix, σ_m vs. strain, internal stress in the matrix, σ_{mi}, vs. strain and thermal stress in the matrix, σ_m^*, vs. strain. From Figure 6 it is evident that the load transfer plays in the case of perpendicular orientation of the fibres plane only negligible role.

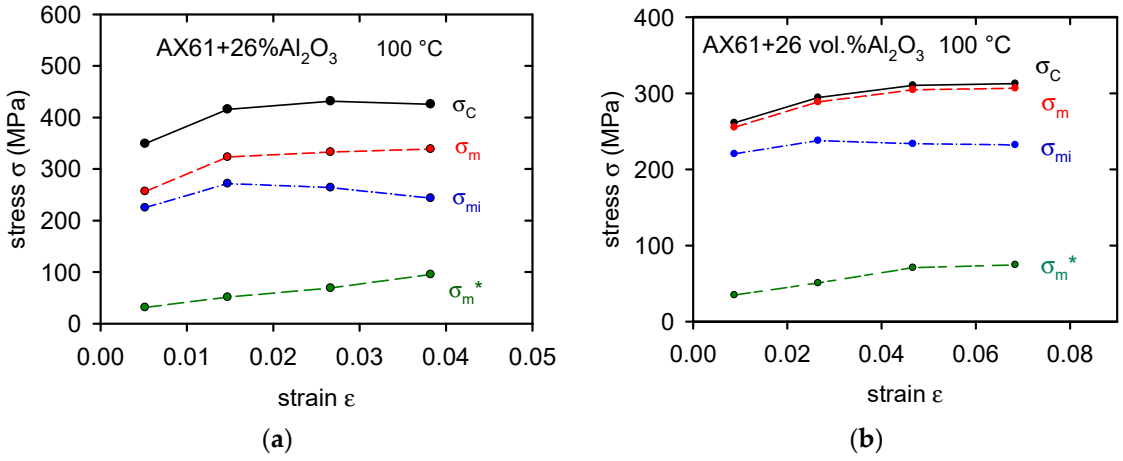

Figure 6. Parts of the stress–strain curves divided into three components estimated for (**a**) parallel and (**b**) perpendicular orientation of the fibres plane. σ_C—deformation stress, σ_m—stress in the matrix, σ_{mi}—internal stress in the matrix, σ_m*—effective stress in the matrix.

Curves for both types of samples in Figure 6 are similar but some differences between them are obvious. Strain to fracture was found to be higher in samples with the perpendicular orientation of the fibre plane, the stress in the matrix is higher in the composite with the parallel orientation. Máthis et al. studied deformation mechanisms in magnesium samples with different grain sizes [55]. They found using acoustic emission measurements that mechanical twinning is a significant deformation mechanism, especially at the beginning of plastic straining.

Composite deformation starts in the matrix by massive twinning [56]. The authors of [56] measured acoustic emission (AE) during compressive deformation of two magnesium alloy-based composites reinforce with Saffil fibres. They estimated two pronounced AE maxima in the early stages of plastic straining. The first peak may be described to the formation of $\{10\bar{1}2\}\langle 10\bar{1}0\rangle$ twins. The second peak came from the twins' production in the system $\{10\bar{1}1\}\langle 10\bar{1}2\rangle$ and generation of dislocations in the vicinity of the yield point. Farkas et al. [47] estimated that the twinned volume at the beginning of plastic deformation was smaller in the sample with the parallel orientation. The twin's boundary is an impenetrable obstacle for dislocation motion [57]. It is very probably the reason for observed higher deformation stresses and strain hardening in the matrix observed in the samples with the parallel orientation.

4.3. Thermally Activated Processes

In the stress relaxation experiments of polycrystalline materials, time dependence of applied (or matrix) stress is observed and so only apparent activation volume may be estimated. This apparent activation volume V is related to the dislocation activation volume, V_D, (measured in monocrystals) as $V = (1/M)V_D$, considering the mobile dislocation density and the internal stress constant. The values of the activation volume are usually presented as a dimensionless quantity, V/b^3. The estimated activation volumes V/b^3 for all samples and temperatures are reported in Figure 7a depending on the thermal stress in the matrix σ_m^*. It can be seen that all values follow one "master curve".

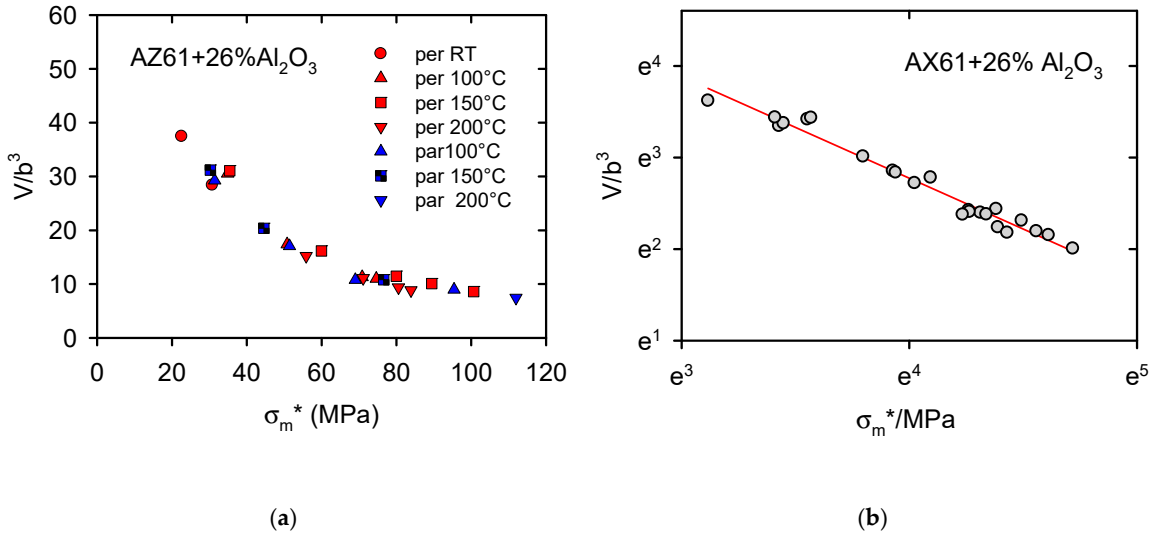

(**a**) (**b**)

Figure 7. Activation volume, V, in b^3 units depending on the thermal stress in the matrix, σ_m^*: (**a**) linear scale, (**b**) bilogarithmic scale.

In thermodynamics, the dislocation (true) activation volume V_D is done by the derivative of the Gibbs free enthalpy:

$$V_d = \left(\frac{\partial \Delta G}{\partial \tau^*}\right)_{T,s} = kT\left(\frac{\partial ln(\dot{\gamma}/\dot{\gamma}_0)}{\partial \tau^*}\right)_{T,s} = \frac{1}{M}kT\left(\frac{\partial ln\left(\dot{\varepsilon}/\dot{\varepsilon}_0\right)}{\partial \sigma^*}\right), \quad (12)$$

where the subscripts T and s indicate that both the temperature and the dislocation microstructure (especially the mobile dislocation density) must be constant during the test.

Kocks et al. [58] suggested an empirical equation between the Gibbs enthalpy, ΔG, and the thermal stress, σ^*, in the following form:

$$\Delta G = \Delta G_0 \left[1 - \left(\frac{\sigma^*}{\sigma_0^*}\right)^m\right]^n \tag{13}$$

where σ_0^* is the stress necessary for dislocation motion through field of local obstacles without the assistance of thermal energy. From (3), (4) and (13), it follows:

$$\sigma^* = \sigma_0^* \left[1 - \left(\frac{kT}{\Delta G_0} \ln \frac{\dot{\varepsilon}_0}{\dot{\varepsilon}}\right)^{1/m}\right]^{1/n}, \tag{14}$$

where m and n are phenomenological parameters described the shape of obstacles. The possible ranges of values m and n are limited by the conditions $0 < m \leq 1$ and $1 \leq n \leq 2$. Ono [59] and Kapoor [60], suggested that Equation (13) with $m = 1/2$, $n = 3/2$ describes a barrier shape profile that fits many predicted barrier shapes. Equation (14) may be rewritten

$$\dot{\varepsilon} = \dot{\varepsilon}_0 \, exp\left[-\frac{\Delta G_0}{kT}\left(1 - \left(\frac{\sigma^*}{\sigma_0^*}\right)^m\right)^n\right] \tag{15}$$

and for the activation volume one obtains:

$$V = kT\frac{\partial ln\dot{\varepsilon}/\dot{\varepsilon}_0}{\partial\sigma^*} = \frac{\Delta G_0 mn}{\sigma_0^*}\left[1 - \left(\frac{\sigma^*}{\sigma_0^*}\right)^m\right]^{n-1}\left(\frac{\sigma^*}{\sigma_0^*}\right)^{n-1} \tag{16}$$

The values of the activation volume should follow the curve given by Equation (16).

Using binominal expansion in Equation (16), the activation volume should depend on the effective stress as $V \propto (\sigma^*)^{-p}$. Estimated values of the activation volumes plotted in bilogarithmic scale are shown in Figure 7b. The slope of this dependence was found to be −1.1. Generally, the values of the power exponent found in the literature vary from −0.5 to −1 [58]. The activation enthalpy $\Delta H = \Delta G - T\Delta S$ (ΔS is the entropy) is done by

$$\Delta H = -TV\left(\frac{\partial\sigma}{\partial T}\right). \tag{17}$$

The activation enthalpy calculated according to (15) for 150 °C gives (1.08 ± 0.05) eV for parallel orientation and (0.94 ± 0.05) eV. High temperature creep was studied on polycrystalline magnesium by McG. Tegart at various stresses and temperatures [61]. He found that the activation energy in a temperature range from room temperature up to $0.6T_m$ (T_m is the melting point in K) is independent of temperature and slightly dependent on the applied stress. Several authors studying thermally activated processes in magnesium and magnesium alloys found activation enthalpy −1 eV [62–65].

The parameters of the thermally activated process (activation enthalpy and activation volume) are typical for certain barriers. Note that their experimental estimation gives the possibility to identify the main barrier relevant for dislocation motion [66]. Magnesium and hexagonal close packed magnesium alloys deform on many several slip systems with dislocations of Burgers vector <a> = $1/3\left[11\bar{2}0\right]$ in basal, prismatic and first kind pyramidal planes and dislocations of Burgers vector <c + a> = $1/3\left[11\bar{2}3\right]$ in first and second pyramidal planes. The main deformation mode in magnesium is basal slip of <a> dislocations. Screw dislocations of Burgers vector $1/3\left[11\bar{2}0\right]$ may glide in nonbasal planes (prismatic and pyramidal of the first kind). Couret and Caillard performed an in situ TEM study of magnesium monocrystals [67,68]. They estimated that the mobility of screw dislocation segments is much lower compared with edge dislocations and their motion is thermally activated. A single controlling mechanism has been identified as the Friedel–Escaig mechanism. This mechanism assumes

a dissociated dislocation on a compact plane (0001) that joints together along a critical length *Lr* producing double kinks on non-compact plane. The activation energy for this process is

$$U = 2U_K + 4U_C + 2U_R \quad (18)$$

where $2U_{K,}$ $4U_C$ and $2U_R$ are the formation energies of the kink pair, of the four constrictions and of the two recombined segments, respectively. The theoretical prediction leads to a value of $2U_K$ superior to 1.2 eV. The activation volume, V, is of the order of d^2b to a few times d^2b, where d is, in this case, the width of the dissociated dislocation [69]. The athermal temperature for this process is estimated as being higher than 700 K. Measurements of temperature relaxation spectrum of internal friction in magnesium showed an internal fiction peak at ~100 °C. This peak was described to screw dislocation motion in non-compact planes [70]. The estimated activation energy ΔH = (1.16 ± 0.05) eV was close to that found in this study. Note that the activation volume of ~17b^3, determined in [69], was estimated for pure magnesium. In an alloy, solute atoms may segregate in the stacking fault and change the width of the dislocation dissociation and so the obstacle width and also the activation volume.

5. Conclusions

Magnesium alloy AX61 reinforced with Saffil short fibres was prepared by squeeze casting into the preform with a 2D fibre array. Deformation and stress relaxation tests performed at elevated temperatures helped us to identify strengthening mechanisms of fibres and thermally activated processes occurring in the deformed matrix. The following conclusions from this complex study can be drawn:

- Saffil fibres reinforced the alloy significantly when the fibre plane was parallel to the stress axis.
- The load transfer (when the fibres plane was parallel to the stress axis) is a significant strengthening mechanism.
- The dislocation density increase due to a significant difference in the thermal expansion coefficient of the matrix and ceramic reinforcement is also important contribution to the strengthening.
- Components of the stress acting in the matrix were estimated at three temperatures.
- All values of the activation volume follow one "master curve" independently on the stress, temperature and orientation of the fibres plane.
- Values of the activation volume of units and tens of b^3 and activation energy of ~ 1 eV indicate that the main thermally activated process is very probably dislocation motion in non-compact planes.

Author Contributions: Z.T. and P.L. conceived and designed the experiments; Z.S. carried out the mechanical tests and microstructure observation; Z.T., P.L., J.D. and Z.D. analysed the data; Z.T. and P.L. wrote the paper. All authors have read and agreed to the published version of the manuscript.

Funding: This research was partly funded by Ministry of Trade and Industry of the Czech Republic within the frame of institutional funding of Long term development of research organizations.

Conflicts of Interest: The authors declare no conflict of interest.

References

1. Advesian, M.M. *ASM Speciality Handbook: Magnesium and Magnesium Alloys*; Advesian, M.M., Baker, H., Eds.; ASM International: Russell Township, OH, USA, 1999.
2. Pekguleryuz, M. Creep Resistant Magnesium Alloys for Power-Train Applications. In *Magnesium Alloys and Their Applications*; Kainer, K.U., Ed.; DGM, Willey-VCH: Weinheim, Germany, 2003; pp. 65–85.
3. Ninomiya, J.R.; Ojiro, T.; Kubota, K. Improved heat resistance of Mg-Al alloys by the Ca addition. *Acta Metall.* **1995**, *43*, 669–674. [CrossRef]
4. Gjestland, H.; Nussbaum, G.; Regazzoni, G.; Lohne, O.; Bauger, Ø. Stress-relaxation and creep behaviour of some rapidly solidified magnesium alloys. *Mater. Sci. Eng. A* **1991**, *134*, 1197–1200. [CrossRef]

5. Terada, Y.; Ishimatsu, N.; Sota, R.; Sato, T.; Ohor, K. Creep Characteristic of Ca-Added Die-Cast AM50 Magnesium Alloys. *Mater. Sci. Forum* **2003**, *419–422*, 459–464.
6. Wenwen, D.; Yangshan, S.; Xuegang, M.; Feng, X.; Min, Z.; Dengyun, W. Microstructure and mechanical properties of Mg-Al based alloy with calcium and rare earth additions. *Mater. Sci. Eng. A* **2003**, *356*, 1–7. [CrossRef]
7. Luo, A.A. Magnesium casting technology for structural applications. *J. Magnes. Alloys* **2013**, *1*, 2–22. [CrossRef]
8. Pekguleryuz, M.; Celikin, M. Creep resistance in magnesium alloys. *Int. Mater. Rev.* **2010**, *55*, 197–217. [CrossRef]
9. Liu, M.; Wang, Q.; Liu, Z.; Wang, G.; Wu, G.; Zhu, Y.; Ding, W. Behavior of Mg-Al-Ca alloy during solution heat treatment at 415 °C. *J. Mater. Sci. Lett.* **2002**, *21*, 1281–1283. [CrossRef]
10. Jiang, B.; Liu, W.; Qiu, D.; Zhang, M.X.; Pan, F. Grain refinement of Ca addition in a twin-roll-cast Mg-3Al-1Zn alloy. *Mater. Chem. Phys.* **2012**, *133*, 611–616. [CrossRef]
11. Chen, Y.; Liu, H.; Ye, R.; Liu, G. Effect of the addition of Ca and Sb on the microstructure and mechanical properties of AZ91 magnesium. *Mater. Sci. Eng. A* **2013**, *587*, 262–267. [CrossRef]
12. Trojanová, Z.; Lukáč, P. Physical aspects of plastic deformation in Mg-Al alloys with Sr and Ca. *Int. J. Mater. Res.* **2009**, *100*, 270–276. [CrossRef]
13. Luo, A.A. Recent magnesium alloy development for elevated temperature applications. *Int. Mater. Rev.* **2004**, *49*, 13–30. [CrossRef]
14. Pekguleryuz, M.O.; Kaya, A.A. Creep Resistant Magnesium Alloys for Powertrain Applications. *Adv. Eng. Mater.* **2003**, *5*, 866–878.
15. Luo, A.A.; Powell, B.R.; Sachdev, A.K. Computational phase equilibrium and experimental investigation of magnesium-aluminium-calcium alloys. *Intermetallics* **2012**, *24*, 22–29. [CrossRef]
16. Elamani, H.A.; Incesu, A.; Korgiopoulus, K.; Pekguleryuz, M.; Gungor, A. Phase selection and mechanical properties of permanent mold cast alloys and the role of Ca/Al ratio. *J. Alloys Compd.* **2018**, *764*, 216–225. [CrossRef]
17. Krajňák, T.; Minárik, P.; Gubicza, J.; Máthis, K.; Kužel, R.; Janeček, M. Influence of equal channel angular pressing routes on texture, microstructure and mechanical properties of extruded AX41 magnesium alloy. *Mater. Charact.* **2017**, *123*, 282–293. [CrossRef]
18. Krajňák, T.; Minárik, P.; Stráská, J.; Gubicza, J.; Máthis, K.; Janeček, M. Influence of equal channel angular pressing on texture, microstructure and mechanical properties of extruded AX41 magnesium. *J. Alloys Compd.* **2017**, *705*, 273–282. [CrossRef]
19. Trojanová, Z.; Halmešová, K.; Džugan, J.; Palček, P.; Minárik, P.; Lukáč, P. Influence of strain rate on deformation behaviour of an AX52 alloy processed by equal channel angular pressing (ECAP). *Lett. Mater.* **2018**, *8*, 517–523. [CrossRef]
20. Krajňák, T.; Minárik, P.; Stráský, J.; Máthis, K.; Janeček, M. Mechanical properties of ultrafine-grained AX41 magnesium alloy at room temperature and elevated temperatures. *Mater. Sci. Eng. A* **2018**, *731*, 438–445. [CrossRef]
21. Casati, R.; Vedani, M. Metal matrix composites reinforced by nano particles—A review. *Metal* **2014**, *4*, 65–83. [CrossRef]
22. Chawla, N.; Chawla, K.K. *Metal Matrix Composites*; Springer: New York, NY, USA, 2013.
23. Gupta, M.; Wong, W.L.E. An insight into processing and characteristic of magnesium based composites. In *Magnesium Technology*; Alderman, M., Manuel, M.V., Hort, N., Neelameggham, N.R., Eds.; Springer: Cham, Switzerland, 2014; pp. 419–428.
24. Ye, H.Z.; Liu, X.Y. Review of recent studies in magnesium matrix composites. *J. Mater. Sci.* **2004**, *9*, 6153–6171. [CrossRef]
25. Trojanová, Z.; Lukáč, P.; Száraz, Z.; Drozd, Z. Mechanical and Acoustic Properties of Magnesium Alloys Based (Nano) Composites Prepared by Powder Metallurgical Routs. In *Light Metal Alloys Applications*; Monteiro, W.A., Ed.; InTech: Rijeka, Croatia, 2014; pp. 163–197.
26. Hassan, S.F.; Gupta, M. Development of a novel magnesium-copper based composite with improved mechanical properties. *Mater. Res. Bull.* **2002**, *37*, 377–389. [CrossRef]
27. Xu, Q.; Bassiouny Saleh, A.M.; Li, Y.; Yuan, Y.; Jiang, J.; Ni, C. Enhancement of strength and ductility of SiC_p/AZ91 composites by RD-ECAP processing. *Mater. Sci. Eng. A* **2020**, 138579. [CrossRef]

28. Song-Jeng, H.; Addisu Negash, A. Experimental investigations of effects of SiC contents and severe plastic deformation on the microstructure and mechanical properties of SiCp/AZ61 magnesium metal matrix composite. *J. Mater. Proc. Technol.* **2019**, *272*, 28–39.
29. Aqeel, A.; Song-Jeng, H. Investigation of severe plastic deformation effects on microstructure and mechanical properties of WS2/AZ91 magnesium metal matrix composites. *Mater. Sci. Eng. A* **2020**, *780*, 139211.
30. Sabirov, I.; Kolednik, O.; Valiev, R.Z.; Pippan, R. Equal channel angular pressing of metal matrix composites: Effect on particle distribution and fracture toughness. *Acta Mater.* **2005**, *53*, 4919–4930. [CrossRef]
31. Ramkumar, K.R.; Dinaharan, I. Accumulative Roll Bonding Route for Composite Materials Production. In *Encyklopedia of materials: Composites*; Elsevier: Amsterdam, The Netherlands, 2020.
32. Aikin, R.M., Jr.; Christodoulou, L. The Role of Equiaxed Particles on the Yield Stress of Composites. *Scr. Metall. Mater.* **1991**, *25*, 9–14. [CrossRef]
33. Arsenault, R.J.; Shi, N. Dislocation Generation due to Differences between the Coefficients of Thermal Expansion. *Mater. Sci. Eng.* **1986**, *81*, 175–187. [CrossRef]
34. Ashby, M.F. Criteria for Selecting the Components of Composites. *Acta Metall. Mater.* **1993**, *41*, 1313–1325. [CrossRef]
35. Yeh, Y.H.; Nakashima, H.; Kurishita, H.; Goto, S.; Yoshinaga, H. Threshold stress for high-temperature creep in particle strengthened Al-1.5 vol.% Be alloys. *Mater. Trans. JIM* **1990**, *31*, 284–292. [CrossRef]
36. Delannay, F. Thermal stresses and thermal expansion in MMCs. In *Comprehensive Composite Materials*; Clyne, T.W., Ed.; Elsevier: Amsterdam, The Netherlands, 2000; Volume 3, pp. 341–369.
37. Orowan, E. Problems of plastic gliding. *Proc. Phys. Soc.* **1940**, *52*, 8–22. [CrossRef]
38. Dotsenko, V.I. Stress Relaxation in Crystals. *Phys. Stat. Sol. (b)* **1979**, *93*, 11–43. [CrossRef]
39. Feltham, P. Stress relaxation in magnesium at low temperatures. *Phys. Stat. Sol.* **1963**, *3*, 1340–1346. [CrossRef]
40. Li, J.M.C. Dislocation Dynamics in Deformation and Recovery. *Canad. J. Appl. Phys.* **1967**, *45*, 493–509. [CrossRef]
41. De Batist, R.; Callens, A. On the analysis of stress relaxation experiments. *Phys. Stat. Sol. (a)* **1974**, *21*, 591–595. [CrossRef]
42. Lide, D.R. (Ed.) *Handbook of Chemistry and Physics*, 73rd ed.; CRC Press: Boca Raton, FL, USA, 1992; ISBN 978-0849304736.
43. Armstrong, A.; Codd, I.; Douthwaite, R.M.; Petch, N.J. The plastic deformation of polycrystalline aggregates. *Philos. Mag.* **1962**, *7*, 45–56. [CrossRef]
44. Cáceres, C.H.; Mann, G.E.; Griffiths, J.R. Grain size hardening in Mg and Mg-Zn solid solutions. *Metal Mater Trans* **2011**, *42*, 1950–1959. [CrossRef]
45. Cáceres, C.H.; Lukáč, P. Strain hardening behaviour and the Taylor factor of pure magnesium. *Philos. Mag.* **2008**, *88*, 977–989. [CrossRef]
46. Lavrentev, F.F.; Pokhil, Y.A.; Zolotukhina, I.N. Analysis of Pairwise Dislocation Interaction and its Contribution to Flow Stress during Magnesium Crystal Basal Slip. *Mater. Sci. Eng.* **1978**, *32*, 113–119. [CrossRef]
47. Farkas, G.; Trojanová, Z.; Száraz, Z.; Minárik, P.; Máthis, K. Effect of the fiber orientation on the deformation mechanisms of magnesium-alloy based fiber reinforced composite. *Mater. Sci. Eng. A* **2015**, *643*, 25–31. [CrossRef]
48. Trojanová, Z.; Ferkel, H.; Lukáč, P.; Riehemann, W. Two new high-damping magnesium composites. *Phys. Stat. Sol.* **2007**, *193*, 205–210. [CrossRef]
49. Trojanová, Z.; Száraz, Z.; Lábár, J.; Lukáč, P. Deformation behaviour of an AS21 alloy reinforced by short Saffil fibres and SiC particles. *J. Mater. Process. Technol.* **2005**, *162–163*, 131–138. [CrossRef]
50. Zapletal, J.; Trojanová, Z.; Doležal, P.; Fintová, S.; Knapek, M. Elastic and Plastic Behavior of the QE22 Magnesium Alloy Reinforced with Short Saffil Fibers and SiC Particles. *Metals* **2018**, *8*, 133. [CrossRef]
51. Jiang, Z.; Lian, J.; Yang, D.; Dong, S. An analytical study of the influence of thermal residual stresses on the elastic and yield behaviors of short fiber-reinforced metal matrix composites. *Mater. Sci. Eng. A* **1998**, *248*, 256–275. [CrossRef]
52. Clyne, T.W.; Withers, P.J. *An Introduction to Metal Matrix Composites*; Cambridge University Press: Cambridge, UK, 1993.
53. Lilholt, H. Additive strengthening. In *Deformation of Multi-Phase and Particle Containing Materials, Proceedings of the 4th Risø International Symposium on Metallurgy and Materials Science, Risø, Roskilde, Denmark, 5–9 September*

1983; Bilde-Sørensen, J.B., Hansen, N., Horsewelt, A., Leffers, T., Lilholt, H., Eds.; Risø National Laboratory: Roskilde, Denmark, 1983; pp. 381–392.
54. Trojanová, Z.; Lukáč, P.; Chmelík, F.; Riehemann, W. Microstructural changes in ZE41 composite estimated by acoustic measurements. *J. Alloys Compd.* **2003**, *355*, 113–119. [CrossRef]
55. Máthis, K.; Čapek, J.; Zdražilová, Z.; Trojanová, Z. Investigation of tension-compression asymmetry of magnesium by use of the acoustic emission technique. *Mater. Sci. Eng. A* **2011**, *528*, 5904–5907. [CrossRef]
56. Trojanová, Z.; Száraz, Z.; Chmelík, F.; Lukáč, P. Acoustic emission from deformed magnesium alloy based composites. *Mater. Sci. Eng. A* **2011**, *528*, 2479–2483. [CrossRef]
57. Trojanová, Z.; Máthis, K.; Lukáč, P.; Janeček, M.; Farkas, G. Plastic Properties of a Mg-Al-Ca Alloy Reinforced with Short Saffil Fibers. *Metal. Mater. Trans. A* **2014**, *45*, 29–35. [CrossRef]
58. Kocks, U.F.; Argon, A.S.; Ashby, M.F. *Thermodynamics and Kinetics of Slip*, 1st ed.; Pergamon Press: Oxford, UK, 1975.
59. Ono, K. Temperature Dependence of Dispersed Barrier Hardening. *J. Appl. Phys.* **1968**, *39*, 1803–1806. [CrossRef]
60. Kapoor, R.; Wadekar, S.L.; Chakravartty, J.K. Deformation in Zr-1Nb-1Sn-0.1Fe using stress relaxation technique. *Mater. Sci. Eng. A* **2002**, *328*, 324–333. [CrossRef]
61. Tegart, W.J.M.G. Activation energies for high temperature creep of polycrystalline magnesium. *Acta Metall.* **1961**, *9*, 614–617. [CrossRef]
62. Milička, K.; Čadek, J.; Ryš, P. High temperature creep mechanisms in magnesium. *Acta Metall.* **1970**, *18*, 1071–1082. [CrossRef]
63. Vagarali, S.S.; Langdon, T.G. Deformation mechanism in h.c.p. metals at elevated temperatures—I. Creep behavior of magnesium. *Acta Metall.* **1981**, *29*, 1969–1982. [CrossRef]
64. Vagarali, S.S.; Langdon, T.G. Deformation mechanisms in h.c.p. metals at elevated temperatures—II. Creep behaviour of a Mg-0.8% Al solid solution alloy. *Acta Metall.* **1982**, *30*, 1157–1170. [CrossRef]
65. Trojanová, Z.; Máthis, K.; Lukáč, P.; Németh, G. Chmelík: Internal stress and thermally activated dislocation motion in an AZ63 magnesium alloy. *Mater. Chem. Phys.* **2011**, *130*, 1146–1150. [CrossRef]
66. Evans, A.G.; Rawlings, R.D. The thermally activated deformation of crystalline materials. *Phys. Stat. Sol.* **1969**, *34*, 9–31. [CrossRef]
67. Couret, A.; Caillard, D. An in situ study of prismatic glide in magnesium—I. The rate controlling mechanism. *Acta Metall.* **1985**, *33*, 1447–1454. [CrossRef]
68. Couret, A.; Caillard, D. An in situ study of prismatic glide in magnesium—II. Microscopic activation parameters. *Acta Metall.* **1985**, *33*, 1455–1462. [CrossRef]
69. Caillard, D.; Martin, J.L. *Thermally Activated Mechanisms in Crystal Plasticity*; Pergamon Materials Series 8; Cahn, R.W., Ed.; Pergamon Press, Elsevier: Oxford, UK, 2003.
70. Trojanová, Z.; Lukáč, P.; Weidenfeller, B.; Riehemann, W. Mechanical damping in magnesium prepared by ball milling in medium temperature region. *Kovove Mater.* **2008**, *46*, 249–256.



© 2020 by the authors. Licensee MDPI, Basel, Switzerland. This article is an open access article distributed under the terms and conditions of the Creative Commons Attribution (CC BY) license (http://creativecommons.org/licenses/by/4.0/).